AN ULTRA-WIDEBAND BANDPASS FILTER WITH HIGH RETURN LOSS AND CONTROLLABLE NOTCH BAND

Phirun Kim, Girdhari Chaudhary, and Yongchae Jeong
Division of Electronics and Information Engineering, IT Convergence Research Center, Chonbuk National University, Jeonju, Republic of Korea; Corresponding author: ycjeong@jbnu.ac.kr

Received 11 May 2016

ABSTRACT: *In this paper, an ultra-wideband (UWB) bandpass filter (BPF) with a high return loss and a notch band is proposed. A high return loss and a notch band can be obtained by controlling characteristics impedance of coupled line and length of the shut stubs, respectively. For the validation, the UWB BPF was designed and measured to obtain 20 dB return loss with a notch band at 5.5 GHz. The results presented indicated that the 20 dB return loss is extended from 2.93 to 5.1 GHz and 6.14 to 11 GHz. The maximum return loss and attenuation at the notch band of 5.6 GHz are 2.3 dB and 16 dB, respectively.* © 2016 Wiley Periodicals, Inc. Microwave Opt Technol Lett 58:2922–2926, 2016; View this article online at wileyonlinelibrary.com. DOI 10.1002/mop.30187

Key words: *coupled line; defected ground structure; high return loss; notch band; ultra wideband bandpass filter*

1. INTRODUCTION

Ultra-wideband (UWB) systems have many advantages in many applications. However, an interference with other narrow band communication systems may occur, such as with world interoperability for mobile access (WiMAX, 3.5 GHz) and a wireless local-area network (WLAN) bands (5.2 and 5.8 GHz). Therefore, UWB bandpass filter (BPF) without and with single- and multiple-notched bands was recently investigated to suppress the interference band [1–9]. The multi-mode resonator (MMR) with input/output coupling and stub-loaded MMR were proposed in Refs. [1,2] with a relatively poor stopped band suppression. Thus, parallel coupled line with a slot in the ground [3] and quadruple-mode resonators [4] were introduced with a wide stopped band characteristic. However, there is no notch in the passband to suppress the interference band. To overcome this, single-notch band UWB BPFs were designed using dual stepped-impedance stub-loaded resonators [5] and interdigital coupling structure [6]. An asymmetric coupling strip to produce dual-notch bands by adjusting the physical length of the resonator was mentioned in Ref. [7]. Similarly, a triple- and quad-notched bands UWB BPF using interdigital coupled with multiple-mode resonator and broadside-coupled microstip/coplanar waveguide was introduced in Refs. [8] and [9], respectively. The previous UWB BPF works were focused on harmonics suppression, notch bands, and the circuit size. However, the UWB BPF with a high return loss (typically 20 dB) was not considered due to a realization and limitations of resonator coupling. The high return loss and harmonic suppression of UWB BPF can improve the stability of the system and enhance maximum output power compared with the lower return loss BPF. The defected ground structure (DGS) is one of the techniques to suppress the harmonics band and it was implemented by etching a pattern structured shape on the ground plane [10,11].

This paper investigates a new UWB BPF design method for a high return loss and good stopband attenuation with a notch band. The proposed filter can provide multi-transmission poles in the passband. A dumbbell-shape DGSs are placed at input and output ports to suppression harmonics.

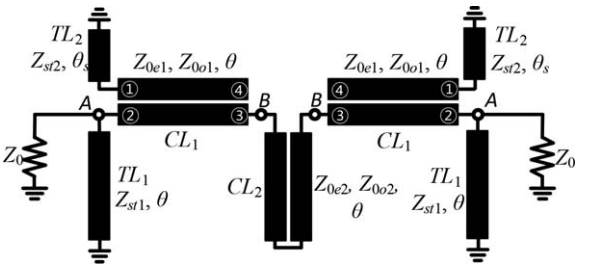

Figure 1 Proposed circuit for UWB bandpass filter with a notch band

2. DESIGN EQUATIONS

Figure 1 shows the proposed structure of the UWB BPF. The proposed circuit consist of three coupled line and four shunt transmission lines with a short stub. Since the proposed network has a symmetrical structure, an even- and odd-mode analysis can be applied. The equivalent circuits for even- and odd-mode excitations are shown in Figures 2(a) and 2(b), respectively. The *S*-parameters can be obtained from input impedance of even- and odd-mode as (1).

$$S_{11}=S_{22}=\frac{Z_{ine}Z_{ino}-Z_0^2}{(Z_{ine}+Z_0)(Z_{ino}+Z_0)} \tag{1a}$$

$$S_{21}=S_{12}=\frac{(Z_{ine}-Z_{ino})Z_0}{(Z_{ine}+Z_0)(Z_{ino}+Z_0)} \tag{1b}$$

For the even-mode, the input impedance Z_{ine} can be expressed as in (2) and (3).

$$Z_{ine}=j\frac{Z_{st1}M_e}{\left(2Z_{0e1}Z_{0o1}\cot\theta-Z_{st2}Z_p\tan\theta_S\right)\left(Z_p-2Z_{0e2}\cot^2\theta\right)+Z_{st1}N_e} \tag{2}$$

where

$$M_e=2Z_{0e1}Z_{0o1}\left(Z_p-2Z_{0e2}\cot^2\theta\right)+Z_{st2}Z_p\tan\theta_S\left(2Z_{0e2}\cot\theta-Z_p\tan\theta\right) \tag{3a}$$

$$N_e=\left(Z_p\cot\theta-2Z_{st2}\tan\theta_S\right)\left(Z_p+2Z_{0e2}\right)-Z_m^2\csc^2\theta\tan\theta \tag{3b}$$

$$Z_P=Z_{0e1}+Z_{0o1} \tag{3c}$$

$$Z_m=Z_{0e1}-Z_{0o1} \tag{3d}$$

From the odd-mode equivalent circuit shown in Figure 2(b), the input impedance Z_{ino} is determined as in (4) and (5).

$$Z_{ino}=j\frac{Z_{st1}M_o}{\left(2Z_{0e1}Z_{0o1}\cot\theta-Z_{st2}Z_p\tan\theta_S\right)\left(Z_p+2Z_{0o2}\right)+Z_{st1}N_o} \tag{4}$$

where

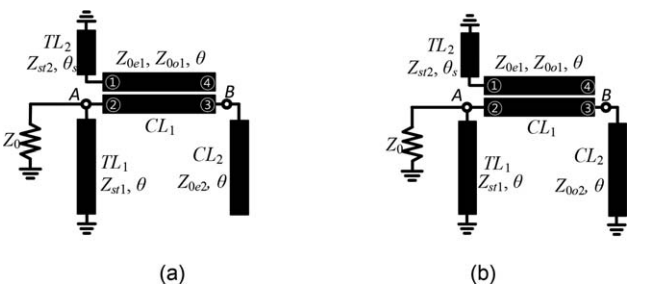

Figure 2 Equivalent circuits of (a) even- and (b) odd-modes

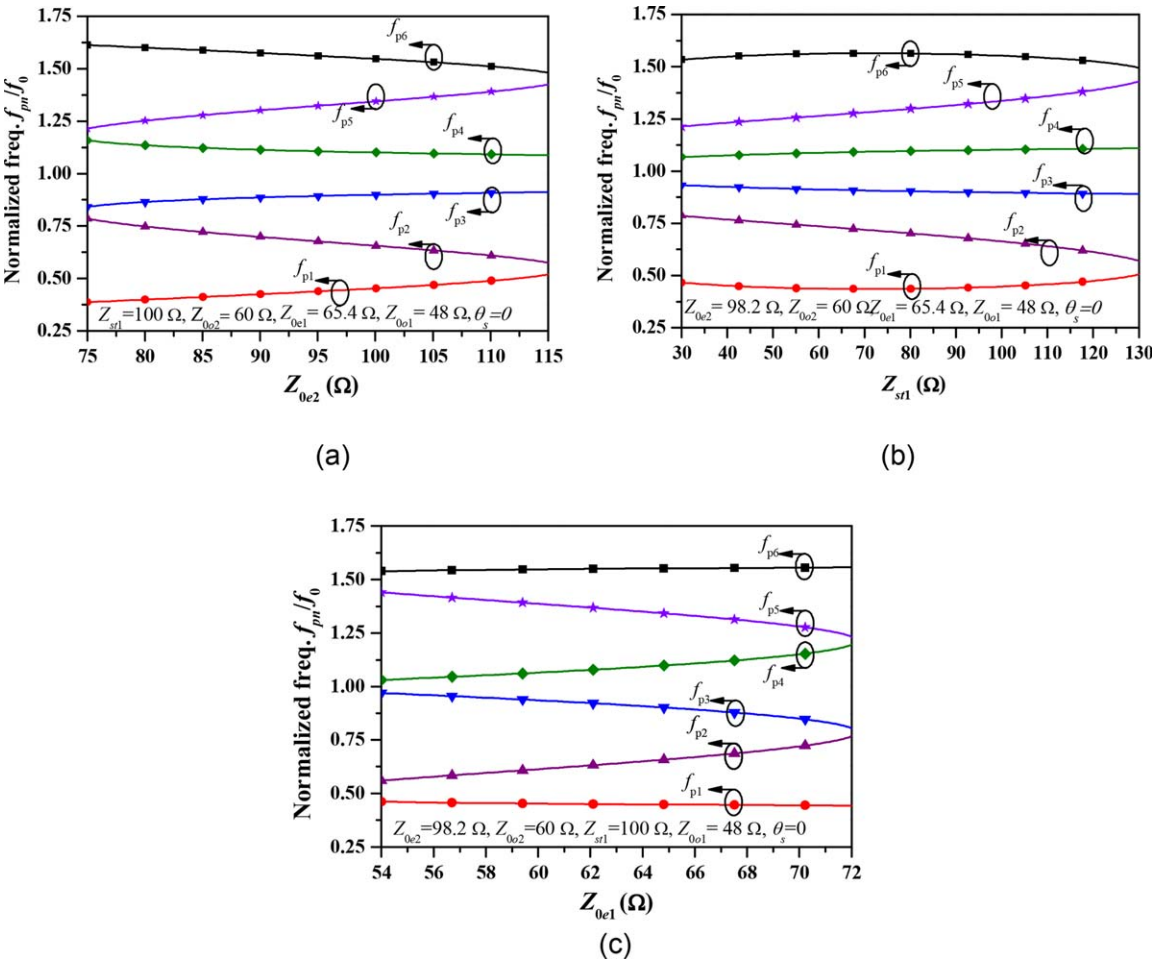

Figure 3 Transmission pole locations according to (a) Z_{0e2}, (b) Z_{st1}, and (c) Z_{0e1}. [Color figure can be viewed at wileyonlinelibrary.com]

$$M_o = \left(2Z_{0e1}Z_{0o1} - Z_{st2}Z_p \tan\theta_S \tan\theta\right)\left(2Z_{0o2} + Z_p\right) \tag{5a}$$

$$N_o = Z_p^2 \cot\theta - \tan\theta\left(Z_m^2 \csc^2\theta + 2Z_pZ_{0o2}\right) + 2Z_{st2}\tan\theta_S\left(2Z_{0o2}\tan^2\theta - Z_p\right) \tag{5b}$$

Equations (2) and (4) indicate that Z_{ine} and Z_{ino} are zero at operating center frequency (f_0) with $\theta_s = 0$. In this condition, the notch band is located at f_0. The locations of the transmission poles (TPs) can be determined according to characteristic impedances of the transmission lines (TLs) and coupled lines. By giving $S_{11} = 0$, the locations of the TPs can be derived as in (6) and (7).

$$\begin{aligned} &-b_4b_7Z_0^2U^3 + \left(b_3b_7Z_0^2 - b_2b_6 + b_4b_8Z_0^2\right)U^2 \\ &+ \left(b_1b_6 - b_7b_5Z_0^2 - b_3b_8Z_0^2\right)U + b_5b_8Z_0^2 = 0 \end{aligned} \tag{6}$$

where

$$b_1 = 2Z_{st1}Z_pZ_{0e1}Z_{0o1} \tag{7a}$$

$$b_2 = 4Z_{st1}Z_{0e1}Z_{0o1}Z_{0e2} \tag{7b}$$

$$b_3 = 2Z_pZ_{0e1}Z_{0o1} - Z_m^2Z_{st1} + Z_pZ_{st1}\left(Z_p + 2Z_{0e2}\right) \tag{7c}$$

$$b_4 = 4Z_{0e1}Z_{0o1}Z_{0e2} \tag{7d}$$

$$b_5 = Z_m^2Z_{st1} \tag{7e}$$

$$b_6 = 2Z_{st1}Z_{0e1}Z_{0o1}\left(Z_p + 2Z_{0o2}\right) \tag{7f}$$

$$b_7 = 2Z_{0e1}Z_{0o1}\left(Z_p + 2Z_{0o2}\right) + Z_p^2Z_{st1} - Z_m^2Z_{st1} \tag{7g}$$

$$b_8 = \left(Z_m^2 + 2Z_pZ_{0o2}\right)Z_{st1} \tag{7h}$$

$$U = \cot^2\theta \tag{7i}$$

$$\frac{f_{pn}}{f_0} = 1 + \left(1 \mp \frac{2}{\pi}\cot^{-1}\sqrt{U}\right) \tag{7j}$$

From the polynomial in (6), three roots of U can be obtained. There are six TPs can be obtained from (7j) and it locate symmetric to f_0. Therefore, the UWB BPF characteristics can be determined by arranging the location of the TPs. Figure 3 shows the location variation of TPs according to Z_{0e2}, Z_{st1}, and Z_{0e1}. As Z_{0e2} increases from 75 Ω to 115 Ω, the first, second, fifth, and sixth TPs (f_{p1}, f_{p2}, f_{p5}, f_{p6}) are changed within the passband. However, the third and fourth TPs (f_{p3}, f_{p4}) are slightly affected at a low Z_{0e2}. Also as Z_{st1} increases from 30 Ω to 130 Ω, the f_{p1}, f_{p2}, f_{p5}, and f_{p6} are changed in different manners. Meanwhile, the f_{p3} and f_{p4} are almost constant. As Z_{0e1} increases from 54 Ω to 72 Ω, the f_{p2}, f_{p3}, f_{p4}, and f_{p5} substantially are changed within the passband. However, the f_{p1} and f_{p6} are slightly affected. The mechanism for the location variation of the TPs according to Z_{0e2}, Z_{st1}, and Z_{0e1} can help the designer to optimize the characteristics of the filter. Figure 4 shows the *S*-parameter characteristics of the UWB BPF with a notch. In

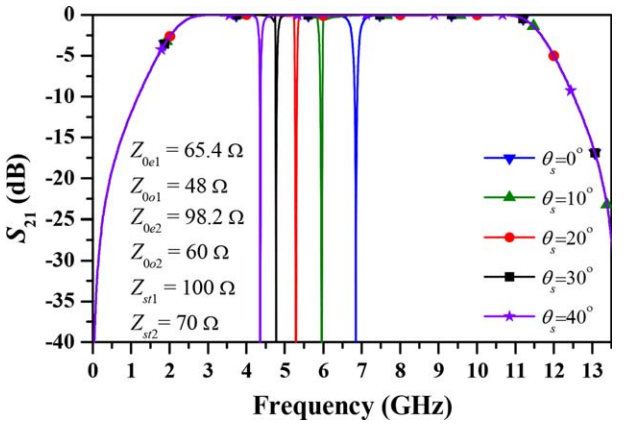

Figure 4 *S*-parameter characteristics of the UWB bandpass filter with notch band. [Color figure can be viewed at wileyonlinelibrary.com]

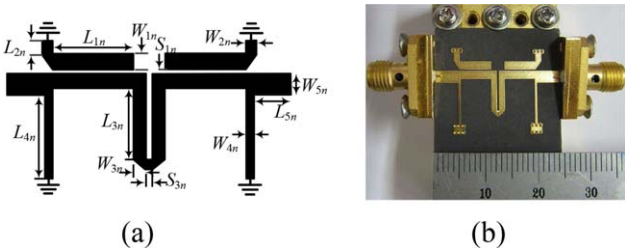

Figure 5 UWB bandpass filter with notch band: (a) EM simulation layout and (b) photograph of fabricated circuit. [Color figure can be viewed at wileyonlinelibrary.com]

TABLE 1 Physical Dimensions of Fabricated UWB Bandpass Filter with Notch Band (Unit: mm)

$W_{1n} = 1.65$	$L_{1n} = 6.25$	$L_{2n} = 1.66$	$L_{3n} = 6.25$	$W_{4n} = 0.45$	$W_{5n} = 2.4$
$S_{1n} = 0.3$	$W_{2n} = 1.16$	$W_{3n} = 1.18$	$S_{3n} = 0.37$	$L_{4n} = 8.1$	$L_{5n} = 4.5$

case of $\theta_s = 0$, the notch band is located at f_0. It is found that the notch band is moved to the lower side from f_0 by increasing θ_s. The characteristic impedances of $Z_{st1} = 100$ Ω, $Z_{0e1} = 65.4$ Ω, $Z_{0o1} = 48$ Ω, $Z_{0e2} = 98.2$ Ω, and $Z_{0o2} = 60$ Ω are chosen to obtain 20 dB return loss. The electrical length of $\theta_s = 17.7°$ should be selected to allocate the notch band at 5.5 GHz.

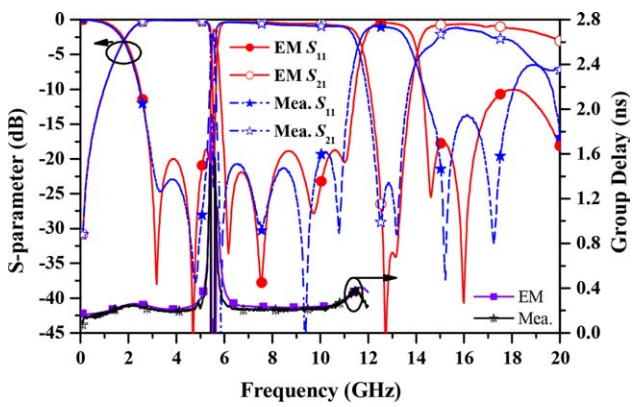

Figure 6 Simulation and measurement results for the UWB bandpass filter with a notch band. [Color figure can be viewed at wileyonlinelibrary.com]

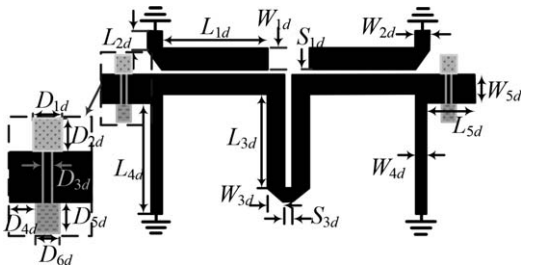

Figure 7 EM simulation layout of proposed DGS UWB bandpass filter with notch band

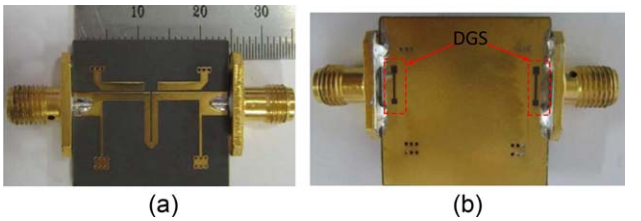

Figure 8 Photograph of the fabricated DGS UWB bandpass filter: (a) top and (b) bottom sides. [Color figure can be viewed at wileyonlinelibrary.com]

TABLE 2 Physical Dimensions of Fabricated UWB Bandpass Filter (Unit: mm)

$W_{1d} = 1.3$	$W_{3d} = 0.91$	$L_{3d} = 6.6$	$W_{4d} = 0.4$	$D_{1d} = 0.9$	$D_{5d} = 0.8$
$S_{1d} = 0.3$	$L_{1d} = 6.5$	$S_{3d} = 0.3$	$L_{5d} = 4.3$	$D_{2d} = 1.1$	$D_{6d} = 0.85$
$W_{2d} = 1.2$	$L_{2d} = 1.55$	$L_{4d} = 6.4$	$W_{5d} = 3.7$	$D_{3d} = 3.7$	$D_{4d} = 1.45$

DGS microstrip line is realized by etching specific patterns in the ground plane and it produce the additional equivalent inductance for the conventional microstrip line. As a result, the transmission line width is broaden. In the proposed structure, the dumbbell-shaped DGSs are placed at the input and output ports and it can provide a wideband rejection to suppress the spurious band [10].

The design steps of the proposed UWB BPF are as follows.

a. Specify f_0, the maximum return loss, and the notch band location.

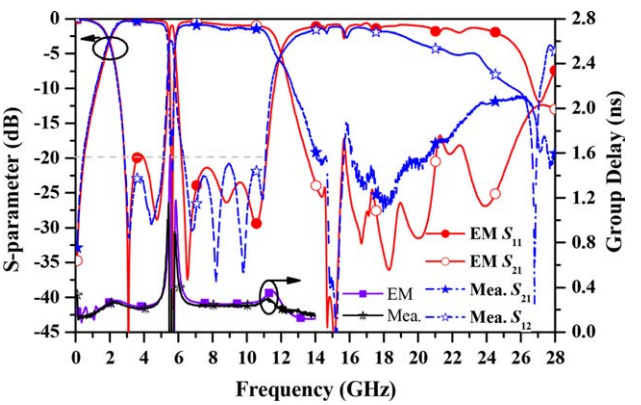

Figure 9 Simulation and measurement result of UWB with DGS. [Color figure can be viewed at wileyonlinelibrary.com]

TABLE 3 Performance Comparison of the Proposed UWB Bandpass Filter with Previous Studies

Refs.	$f0$ (GHz)	IL (dB)	RL (dB)	Notch band	FBW (%)	Selectivity	Upper stopband >15 dB (GHz)	Circuit size, mm × mm	Substrate ε_r/h (mm)
[3]	7	<1	18	No	100	Poor	12.0–26.5	12 × 7	10.2/0.635
[4]	6.9	1.1	10	no	119*	Poor	12–30	NA	10.8/0.635
[5]	7.1	NA	>10	1	110	High	11.1–13	49.3 ×50	2.2/0.787
[6]	8	1	10	1	118*	Poor	13.8–16	15.4 × 3.1	3.5/0.508
[7]	6.9		>12	2	118.84*	Poor	11.9–14	23.6 × 2.7	2.2/0.787
[8]	5.2	0.8	10	3	105.9*	High	8.4–11	41 × 18	3/1.57
[9]	≈6.3	2	13.3	4	≈114.3[c]	High	10.1–15	12.1 × 16.2	2.2/0.508
This work	7.01	1.2	>20	1	115.8	Poor	13.5–22.44	16 × 19	2.2/0.787

*3 dB bandwidth; c, cutoff frequency bandwidth.

b. Calculate TPs using (6)–(7) and then optimize the locations of the TPs.
c. Determine θ_s to allocate the notch band according to the specification.
d. Calculate the physical dimension of the coupled lines and the TLs according to the PCB substrate.
e. Then, the DGS is applied to the UWB BPF for harmonics suppression. Finally optimized UWB BPF characteristic using an electromagnetic (EM) simulator.

3. SIMULATION AND MEASUREMENT RESULTS

Figure 5 depicts the EM simulation layout as well as a photograph of the fabricated UWB BPF with the notch band. The final physical dimensions after optimization using a full-wave EM simulation are shown in Table 1. The size of the fabricated filter is 16 mm × 19 mm. The results of the simulation and measurement results for the *S*-parameters and the group delay are shown in Figure 6. The measurement results are in good agreement with those obtained from the simulations. As can be seen in Figure 6, six TPs are obtained in the passband. The measurement indicates that the insertion and return losses are 0.43 dB and 21.8 dB at $f_0 = 6.85$ GHz, respectively. Similarly, the FBW of the 19 dB return loss is 114.1% extending over 2.98–5.26 GHz and 5.74–10.9 GHz, and the maximum insertion loss is better than 1 dB with the same frequency range. S_{11} and S_{21} are obtained as −2.1 dB and −24 dB at 5.53 GHz, respectively, for the notch band. The maximum group delay in the passband is of 0.23 ns. However, the harmonics suppression is poor.

Two compact asymmetric dumbbell-shape DGSs were used at the input and output ports of the proposed UWB BPF with a notch band to improve the harmonic suppression characteristics. Figures 7 and 8 show the designed layout and photographs of the top and bottom sides of the fabricated circuits, respectively. The final physical dimensions of the full-wave simulation are shown in Table 2. The size of the fabricated filter is 16 mm × 19 mm. The results of the simulation and measurement for the *S*-parameters and the group delay are shown in Figure 9. The measurement results are in good agreement with the simulations. The measured results indicate insertion and return losses of 0.6 dB and 24.7 dB at f_0 =6.85 GHz, respectively. Similarly, a return loss better than 20 dB is extended from 2.93 to 5.1 GHz and 6.14 to 11 GHz, respectively. The measured FBW of the 20 dB return loss is 115.8%. The maximum insertion loss is better than 1.2 dB with the same frequency range. The notch band S_{11} and S_{21} are obtained −2.3 dB and −16 dB at 5.6 GHz, respectively. Moreover, the maximum group delay in the passband is better than 0.29 ns and the group delay variation is less than 0.06 ns. A wide stopband attenuation is better than 15 dB over DC to 0.74 GHz and 13.5 GHz to 22.44 GHz. The performance comparison of the proposed circuit with state-of-arts is summarized in Table 3. The proposed UWB BPF can provide a high return loss with a narrow notch band in addition to wide bandwidth. The high return loss for BPF can improve the overall system performance and stability. Moreover, the proposed UWB BPFs provide a flatness and a low group delay in the passband. Even though the proposed UWB BPF shows relatively poor frequency selectivity, this selectivity can be improved by using several DGSs. In this case, the trade-off between frequency selectivity and circuit size is required.

4. CONCLUSION

In this paper, a new UWB bandpass filters with high return loss was proposed. The notch band located within the UWB passband can be controlled by adjusting the length of the shunt transmission line and does not affect the passband performance. Defected ground structures are used to improve the spurious characteristic at the second harmonic band. The high return loss and the harmonic suppression characteristics of the proposed UWB bandpass filter can improve the overall system performance and stability.

REFERENCES

1. L. Chen, C. Lee, and C.G. Hsu, Novel UWB BPF design using modified trisection MMR, Microw Opt Technol Lett 50 (2013), 2904–2907.
2. R. Li and L. Zhu, Compact UWB bandpass filter using stub-loaded multiple-mode resonator, IEEE Microw Wireless Compon Lett 17 (2007), 40–42.
3. A. Abbosh, Design method for ultra-wideband bandpass filter with wide stopband using parallel-coupled line microstrip lines, IEEE Trans Microw Theory Tech 60 (2012), 31–38.
4. S. Wong and L. Zhu, Quadruple-mode UWB bandpass filter with improved out-of-band rejection, IEEE Microw Wireless Compon Lett 19 (2009), 152–154.
5. S. Oh, B. Shin, J. Jeong, and J. Lee, A UWB bandpass filter with a notched band using dual stepped-impedance stub-loaded resonators, Microw Opt Technol Lett 56 (2014), 1785–1787.
6. K. Xu, Y. Zhang, J. Lewei, W.T. Joines, and Q. Huo, Miniaturized notch-band UWB bandpass filters using interdigital-coupled feedline structure, Microw Opt Technol Lett 56 (2014), 2215–2217.
7. K. Song and Q. Xue, Compact ultra-wideband (UWB) bandpass filters with multiple notched bands, IEEE Microw Wireless Compon Lett 20 (2010), 447–449.
8. C. Chiang, J. Xu, and J. Liu, Compact ultrawideband bandpass filter with triple notched-bands and sharp transmission zeros based on CSRR, DGS, and FMRR configurations, Microw Opt Technol Lett 56 (2014), 2324–2330.

9. X. Luo, J.G. Ma, K. Yeo, and E. Li, Compact ultra-wideband (UWB) bandpass filter with ultra-narrow dual- and quad-notched bands, IEEE Trans Microw Theory Tech 59 (2011), 1509–1519.
10. G. Chaudhary, Y. Jeong, and J. Lim, Dual-band bandpass filter with independently tunable center frequencies and bandwidths, IEEE Trans Microw Theory Tech 61 (2013), 107–116.
11. J. Lim, C. Kim, D. Ahn, Y. Jeong, S. Nam, Design of low-pass filters using defected ground structure, IEEE Trans Microw Theory Tech 53 (2005), 2539–2545.

A COMPACT CIRCULARLY-POLARIZED GPS ANTENNA USING LTCC TECHNOLOGY

Jamal Zaid, M. Farahani, and Tayeb A. Denidni
Place Bonaventure 800, de La Gauchetière Ouest Portail Nord-Ouest, bureau 6900 Montreal, Quebec H5A 1K6, Canada;
Corresponding author: jamal.zaid@emt.inrs.ca

Received 11 May 2016

ABSTRACT: *A circularly-polarized GPS antenna for L1 (1575 MHz) is designed and fabricated using low temperature cofired ceramic (LTCC) technology. A parallel patch and high dielectric constant composite ceramic with LTCC fabrication method are employed to design a compact structure. The electrical connected parallel patch interval and size are the main parameters for achieving resonance frequency at L1-band to support modern GPS coding schemes. The proposed electrically connected upper and lower patches are connected together with vertical via pins and therefore did not have any connection with the ground plane. By embedding a truncated corner patch and rectangular slots to this design, the right-hand circularly-polarized (RHCP) field property is achieved. By using these features, a compact simple CP-GPS antenna with 2.32 dBic gain at 1575 MHz is designed and fabricated. The proposed antenna has a total compact size of 15 × 15× 4 mm^{3}and operates over the frequency band from 1570 to 1585 MHz for* VSWR < 2.
 Microwave Opt Technol Lett 58:2926–2930, 2016; View this article online at wileyonlinelibrary.com. DOI 10.1002/mop.30183

Key words: *low temperature cofired ceramic; global positioning system; patch antenna; circularly polarized antenna*

1. INTRODUCTION

Since the last decades, the development of global positioning system (GPS) in commercial applications, such as localization through mobile devices and phones, vehicle navigation systems, and industrial scale asset tracking, has attracted much incentives for designing compact GPS antennas with high performance and small size [1–8]. Because of the operating frequency at 1575 MHz for GPS module, the antenna size is the limiting factor. The weak signal level of the GPS makes it vulnerable to intentional or unintentional jammers. In military communication systems this drawback is solved by employing GPS arrays to produce nulls in the directions of the jamming signals. In recent years, various antennas with different techniques, such as folding and meandering, have been proposed for GPS systems drawbacks [8,9]. Using (LTCC) technology for easy integration and flexible via distribution anywhere in the substrate, has emerged as a novel method for designing compact and lightweight antennas. Additionally in wireless communications, circularly polarized (CP) antennas are getting popular to enhance the system performance; they can provide better mobility and deeper weather penetration than linearly polarized (LP) antennas, and easier deployment of transmitter and receiver without causing any polarization mismatch [9–11]. Some of the previous reported techniques that have been used to design CP-GPS antennas are stated as: Embedding stacked patch designs for dual-band operation [7,12], shaped patches [8], and embedding slot loaded patches as radiation elements [13].

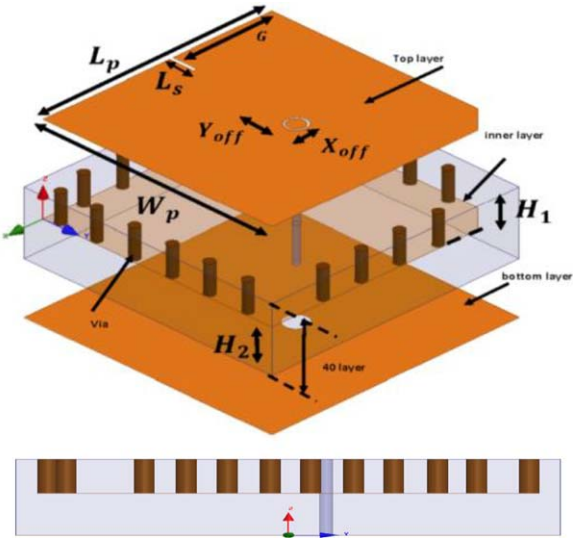

Figure 1 Geometry of the proposed CP-GPS patch antenna. [Color figure can be viewed at wileyonlinelibrary.com]

However, these antenna designs have some major drawbacks related to noncompactness, bulkiness, and difficulty in fabrication. For this reason, we have restricted ourselves to design compact circularly polarized elements in this work. Therefore, in this perspective a compact CP-GPS antenna design using low temperature cofired ceramic technology has emerged new attempts to address physical size, electrical characteristics, and scalability, easily redesigned for other frequencies.

In this letter, we propose a compact circularly polarized patch GPS antenna (L1: 1575 MHz) designed by using LTCC technology, which is only 14 × 14 mm^2 in size and 4 mm in thickness. In the following sections, the antenna design and obtained result are described and discussed.

2. COMAPCT L1-BAND GPS ANTENNA DESIGN

Figure 1 shows the geometry of the proposed GPS antenna. It is composed of three parallel layers and via holes. The top layer includes a truncated patch and a rectangular slot to achieve a good right hand circular polarization, the antenna is fabricated on a composite ceramic LTCC type system with a fired thickness of 0.1 mm for each layer (40 layers). The composite ceramic has a dielectric permittivity of 68, loss tangent of 0.003 and thickness of 4 mm. However, all metal layers are silver plated, but the top and bottom layers can plated with gold to reduce surface roughness and oxidation. Considering the proposed antenna performance, a top and inner patches and via holes between them are proposed to have 10 × 12 mm and 1.8 mm dimensions, respectively. The performances of the CP-GPS antenna were investigated using Ansoft HFSS (ver.15). During the simulation process to keep the bandwidth unchanged and assessments for the sensitivity of the antenna performance, ±0.15 mm variation tolerance to via hole radius of the antenna structure is added, and the effect of fabrication errors is considered. In this structure, the probe is connected to the main patch